



## TCMHTI: a Transformer-based herb-target interaction prediction model for Qingfu Juanbi Decoction in rheumatoid arthritis

Zhenzhong LIANG<sup>a</sup>, Changsong DING<sup>a, b\*</sup>

*a. School of Informatics, Hunan University of Chinese Medicine, Changsha, Hunan 410208, China*

*b. Big Data Analysis Laboratory of Traditional Chinese Medicine, Hunan University of Chinese Medicine, Changsha, Hunan 410208, China*

### ARTICLE INFO

#### Article history

Received 06 November 2024

Accepted 23 April 2025

Available online 25 June 2025

#### Keywords

Transformer

Qingfu Juanbi Decoction

Rheumatoid arthritis

Deep learning

Network pharmacology

### ABSTRACT

**Objective** To predict the potential targets of Qingfu Juanbi Decoction (青附蠲痹汤, QFJBD) in treating rheumatoid arthritis (RA) using an improved Transformer model and investigate the network pharmacological mechanisms underlying QFJBD's therapeutic effects on RA.

**Methods** First, a traditional Chinese medicine herb-target interaction (TCMHTI) model was constructed to predict herb-target interactions based on Transformer improvement. The performance of the TCMHTI model was evaluated against baseline models using three metrics: area under the receiver operating characteristic curve (AUC), precision-recall curve (PRC), and accuracy. Subsequently, a protein-protein interaction (PPI) network was built based on the predicted targets, with core targets identified as the top nine nodes ranked by degree values. Gene Ontology (GO) functional and Kyoto Encyclopedia of Genes and Genomes (KEGG) pathway enrichment analyses were performed using the targets predicted by TCMHTI and the targets identified through network pharmacology method for comparison. Then, the results were compared. Finally, the core targets predicted by TCMHTI were validated through molecular docking and literature review.

**Results** The TCMHTI model achieved an AUC of 0.883, PRC of 0.849, and accuracy of 0.818, predicting 49 potential targets for QFJBD in RA treatment. Nine core targets were identified: tumor necrosis factor (TNF)- $\alpha$ , interleukin (IL)-1 $\beta$ , IL-6, IL-10, IL-17A, cluster of differentiation 40 (CD40), cytotoxic T-lymphocyte-associated protein 4 (CTLA4), IL-4, and signal transducer and activator of transcription 3 (STAT3). The enrichment analysis demonstrated that the TCMHTI model predicted 49 targets and enriched more pathways directly associated with RA, whereas classical network pharmacology identified 64 targets but enriched pathways showing weaker relevance to RA. Molecular docking demonstrated that the active molecules in QFJBD exhibit favorable binding energy with RA targets, while literature research further revealed that QFJBD can treat RA through 9 core targets.

**Conclusion** The TCMHTI model demonstrated greater accuracy than traditional network pharmacology methods, suggesting QFJBD exerts therapeutic effects on RA by regulating targets like TNF- $\alpha$ , IL-1 $\beta$ , and IL-6, as well as multiple signaling pathways. This study provides a novel framework for bridging traditional herbal knowledge with precision medicine, offering actionable insights for developing targeted TCM therapies against diseases.

\*Corresponding author: Changsong DING, E-mail: dingcs1975@hnuem.edu.cn.

Peer review under the responsibility of Hunan University of Chinese Medicine.

DOI: 10.1016/j.dcmcd.2025.05.007

**Citation:** LIANG ZZ, DING CS. TCMHTI: a Transformer-based herb-target interaction prediction model for Qingfu Juanbi Decoction in rheumatoid arthritis. Digital Chinese Medicine, 2025, 8(2): 206-218.

## 1 Introduction

Rheumatoid arthritis (RA) is a systemic autoimmune disease primarily affecting joints, and in several cases, it can lead to disability [1]. In traditional Chinese medicine (TCM), RA is classified as Bi (痹) syndrome [2]. TCM practitioners have developed an extensive understanding of Bi syndrome over two millennia of practice, and based on this knowledge, numerous classical formulas have been created. Qingfu Juanbi Decoction (青附蠲痹汤, QFJBD), derived from the classical formula Wutou Decoction (乌头汤), includes Fuzi (Aconiti Lateralis Radix Praeparata), Qingfengteng (Sinomenii Caulis), Huangqi (Astragali Radix), Baishao (Paeoniae Radix Alba), and Mudanpi (Moutan Cortex), which can significantly alleviate RA symptoms, such as joint swelling, pain, and limited flexion and extension [3]. However, the mechanisms underlying the effects of QFJBD on RA remain partially understood, impeding the advancement of clinical applications.

Drug-target interaction (DTI) experiments have been conducted to explore and explain the mechanisms of TCM. Due to the multi-component and multi-target nature of TCM, current DTI experiments are quite costly and time-consuming, making it difficult to identify active compounds and their corresponding biological targets [4]. Therefore, network pharmacology has been increasingly applied in TCM as a promising alternative [5], offering the potential to address the limitations of expensive and time-consuming DTI experiments. To some extent, the network of “drug-target-disease” relationships in network pharmacology aligns with the multi-component and multi-target properties of TCM [6]. However, the accuracy of network pharmacology predictions is often compromised by incomplete information on herbal components [7].

With the substantial advancement of computer science, machine learning has shown great potential applicability in DTI prediction. However, traditional machine learning approaches are often limited by their heavy reliance on manual feature engineering, which increases the complexity of model development and may lead to the unexpected exclusion of crucial information [8]. In contrast to traditional machine learning, deep learning methods, with powerful feature learning capabilities, can automatically extract high-level abstract features from raw data and effectively bypass the tedious process of manual feature design. More importantly, deep learning models possess superior abilities in nonlinear fitting, allowing them to capture complex interaction patterns between drugs and targets and reveal hidden associations, something traditional methods struggle to achieve [9]. Thus, deep learning demonstrates significant superiority in DTI prediction.

Currently, most deep learning-based DTI prediction tasks focus on western drug-target interactions. In

contrast, TCM consists of numerous components that cannot be represented by a single active compound. The theory of TCM defines the properties of herbs based on dimensions such as nature, flavor, meridian tropism, and toxicity. Previous research has shown that when herbs are quantified into 23-dimensional vectors based on these properties, herbs with similar efficacies are closer in Euclidean space [10]. Therefore, this study quantifies herbs into 23-dimensional vectors. Due to the lack of structural information for many proteins, amino acid sequences are used as the initial representation of targets. The Transformer model [11], proposed by the Google team, was applied in this study because both herb and target representations are in sequence form. The Transformer is powerful for processing sequence information, utilizing a self-attention mechanism instead of the recurrent neural network (RNN) structure commonly used in natural language processing tasks [12]. However, previous Transformer models are generally used for sequence-to-sequence regression, making them unsuitable for DTI prediction. The TransformerCPI model [13], modified based on the Transformer for DTI prediction tasks, has achieved promising results by training protein sequences as text. However, on one hand, the encoder integrates one-dimensional convolutional neural networks and gated units. Further work is needed to improve convolutional neural networks for sequence tasks, such as using RNN, long short-term memory (LSTM), and other models targeting sequence tasks [14]. On the other hand, the TransformerCPI model focuses solely on compound-protein interaction prediction, which does not apply to TCM tasks.

As summarized, we propose a TCM herb-target interaction (TCMHTI) model to predict potential targets of QFJBD in treating RA and conduct enrichment analysis using the predicted targets to investigate the network pharmacological mechanisms of QFJBD in RA treatment.

## 2 Materials and methods

Inspired by the TransformerCPI model, this study proposes the TCMHTI model, an improved version of the Transformer, to extract features from the 23-dimensional herb vectors and target sequences and predict their interactions. Then, protein-protein interaction (PPI) analysis was performed on the positively interacting targets predicted by TCMHTI, and potential core targets were screened based on degree values. To further explore the mechanism of QFJBD in treating RA and validate the superiority of the TCMHTI method, enrichment analysis was conducted on the targets predicted by the TCMHTI model. Subsequently, the classical network pharmacology method was used to screen the intersection targets of QFJBD herb components acting on RA. Enrichment analysis was also performed on these intersection targets. The

results of both analyses were compared and analyzed, supplemented by molecular docking and literature validation of the accuracy of TCMHTI-predicted targets.

## 2.1 Dataset preparation

Data on herbs, compounds, and targets were collected from the Traditional Chinese Medicine Systems Pharmacology Database and Analysis Platform (TCMSP; <http://www.tcm-sp-e.com>) and the Traditional Chinese Medicine Integrated Database (TCMID; <http://www.megabionet.org/tcmid/>). The data were filtered based on oral bioavailability (OB)  $\geq 30\%$  and drug-likeness (DL)  $\geq 0.18$  [15]. Herb-target pairs collected from TCMSP and TCMID were used as the positive sample set for this study. The negative sample set was generated using the following methods. First, the herb-target pairs in the positive sample set were separated, and duplicates were removed. Second, herbs and targets were randomly re-paired, and duplicate pairs in the positive sample set were eliminated. Third, approximately 1.5 times the number of positive sample pairs was randomly selected to form the negative sample set. The positive and negative sample sets were randomly shuffled and combined to create the total training dataset for this study. RA target data were retrieved from DisGeNET (score\_gda  $\geq 0.5$ ) and GeneCards (relevance\_score  $\geq 40$ ) databases using “rheumatoid arthritis” as the keyword. Subsequently, the predicted targets were combined in a whole permutation with the five herbs of QFJBD, forming a dataset of herb-target interactions. In total, two datasets were collected: a training dataset for TCMHTI model development and a prediction dataset for target identification using the trained model. The data are shown in Table 1.

**Table 1** Herb-target interactions dataset

Dataset	Herb	Target	Interaction	Positive	Negative
Training	803	4 049	54 391	22 274	32 117
Prediction	5	57	285	null	null

## 2.2 TCMHTI model architecture

The TCMHTI model maintains the encoder-decoder structure of the Transformer as shown in Figure 1. Two types of inputs are included in the TCMHTI model: target vectors and herb vectors. For targets, amino acid sequences were collected and mapped to low-dimensional real-valued target feature vectors using the Word2Vec model [16]. Specifically, the amino acid sequences were divided into multiple 3-gram sequences. With these 3-gram sequences, we formed a precursor library, which was trained into word vectors using Word2Vec. Negative sampling was used in training the word vector representations, and the following objective function was used in the calculation:

$$\arg \max_{\theta} \prod_{(w, c) \in D} p(D = 1 | c, w; \theta) \prod_{(w, c) \in D'} p(D = 0 | c, w; \theta) \quad (1)$$

where  $(w, c)$  represents the set of all word-context pairs.  $D$  is the positive sample training dataset, and  $D'$  is the negative sample training dataset.  $p(D = 1 | c, w; \theta)$  is the probability that  $(w, c)$  pairs came from the training data.  $p(D = 0 | c, w; \theta)$  is the probability that  $(w, c)$  did not come from the training data. The probability  $p(D = 1 | w, c; \theta)$  is defined by applying a sigmoid function to the word vectors.

$$p(D = 1 | w, c; \theta) = 1 / (1 + e^{-V_c \cdot V_w}) \quad (2)$$

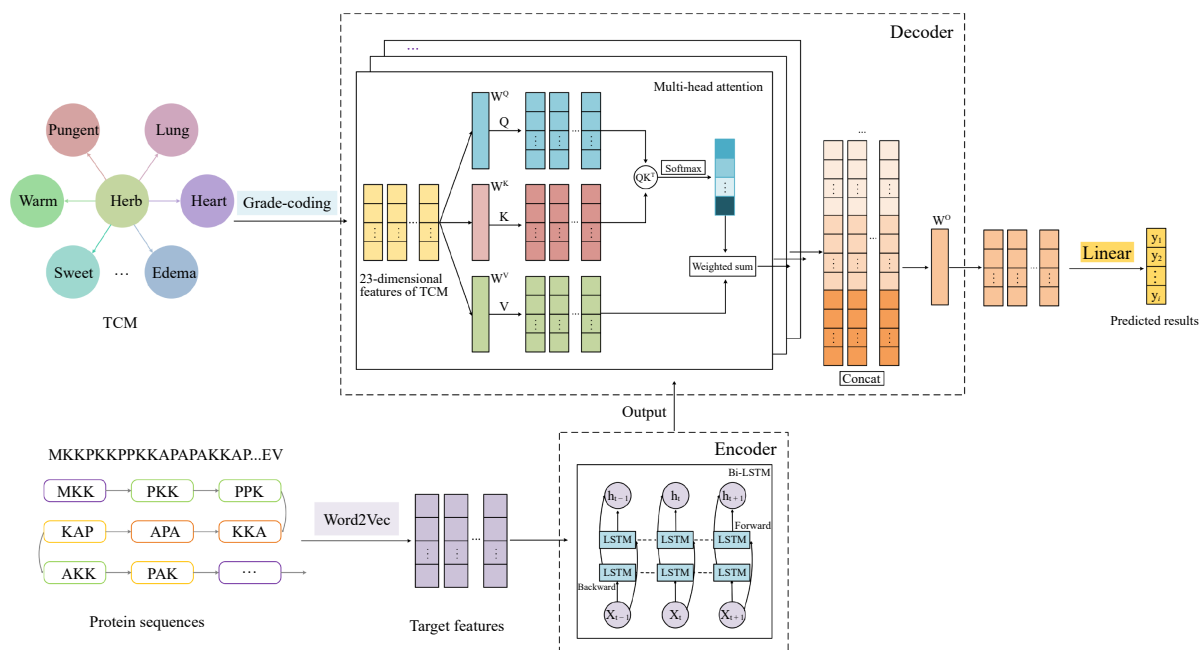


**Figure 1** TCMHTI model architecture diagram

In this context, the parameter  $\theta$  represents the word vectors we trained within the optimization framework.  $v_c$  and  $v_w$  are the vector representations of the context  $c$  and the word  $w$ , respectively. In training the embedding vectors, we set each 3-gram as a 100-dimensional vector.

For herbs, their attributes such as Siqi (四气, four natures), Wuwei (五味, five flavors), and toxicity were measured using exponential quantitative scales. Examples of partial herb vectors are shown in Table 2. In the TCMHTI encoder, the multi-head self-attention mechanism layer was replaced with a bidirectional long short-term memory (Bi-LSTM) network [14]. This modification reduced the model's complexity, making it more suitable for the small to medium-sized herb-target datasets in this study. Moreover, Bi-LSTM performed excellently in processing sequence data and effectively prevented gradient vanishing and exploding compared with other RNN models.

For the decoder, position embedding and masking operations irrelevant to the DTI prediction task were removed, but the multi-head self-attention mechanism layer remained. The multi-head self-attention mechanism layer is a key technical component of the Transformer. The input sequence is represented as three matrices: the query matrix ( $Q$ ), the key matrix ( $K$ ), and the value matrix ( $V$ ). If  $H_i$  is assumed as the input sequence, the matrices are represented as follows:

$$Q_i = W_Q H_i \quad (3)$$

$$K_i = W_K H_i \quad (4)$$

$$V_i = W_V H_i \quad (5)$$

$W_Q$ ,  $W_K$ , and  $W_V$  are the weight matrices for query, key, and value, respectively.

Then, a score matrix  $S_i$  can be obtained, which indicates the relevance of each query to each key by calculating the dot product between the query matrix and the key matrix:

$$S_i = Q_i K_i^T \quad (6)$$

Following that, the self-attention output matrix  $Z_i$  can be obtained by normalizing the score matrix  $S$  and

weighting it with the value matrix value:

$$Z_i = \text{softmax}(S_i / \sqrt{d_k}) \cdot V_i \quad (7)$$

$d_k$  is the dimension of the key matrix. The softmax function normalizes each score into a probability distribution, which is then multiplied by the value matrix to obtain the output matrix.

The vectorized target  $T$  was input into the encoder and processed through the Bi-LSTM layer to get a feature-enriched target feature vector  $T'$ . Subsequently, the herb vector  $H_i$  was an input into the decoder and entered the multi-head self-attention layer with the target feature vector  $T'$  to extract interaction information between the herb and the target. The decoder outputted an interaction feature vector  $x_i$ , and the norm of the vector was calculated:

$$x'_i = \|x_i\|_2^2 \quad (8)$$

The weight of each vector can be calculated by the softmax as follows:

$$\alpha_i = \exp(x'_i) / \sum_{i=1}^a \exp(x'_i) \quad (9)$$

$a$  represents the number of vectors. The final interaction feature vector  $y_i$  is calculated through the weighted sum of the interaction vector  $x'_i$  and the vector weight  $\alpha_i$ :

$$y_i = \sum_{i=1}^a \alpha_i x'_i \quad (10)$$

Finally, the output passed through a fully connected layer to generate the prediction result. As this is a binary classification task, a binary cross-entropy loss function was employed to train the model, formulated as follows:

$$\text{Loss}_i = -[y_i \log \hat{y}_i + (1 - y_i) \log(1 - \hat{y}_i)] \quad (11)$$

The model prediction results were classified into two categories: 1 for interaction and 0 for no interaction. Herb-target pairs with predicted scores  $\geq 0.5$  were classified as interacting (positive), while those with scores  $< 0.5$  were considered non-interacting (negative).

**Table 2** Examples of herb vectors

Herb	Herb vector
Baishao (Paeoniae Radix Alba)	[0.5, 0, 0, 0, 0, 1, 1, 0, 0, 0, 0, 0, 0, 0, 0, 0, 0, 0, 0, 0, 1, 1, 0, 0]
Fuzi (Aconiti Lateralis Radix Praeparata)	[0, 1, 0, 0, 0, 0, 0, 1, 1, 0, 0, 0, 1, 0, 0, 0, 0, 0, 0, 0, 1, 0, 1, 2]
Huangqi (Astragali Radix)	[0, 0, 0.5, 0, 0, 0, 0, 1, 0, 0, 1, 0, 0, 0, 0, 0, 0, 0, 0, 0, 1, 0, 0, 0]
Mudanpi (Moutan Cortex)	[0.5, 0, 0, 0, 0, 0, 1, 0, 1, 0, 0, 0, 1, 0, 0, 0, 0, 0, 0, 0, 0, 1, 1, 0]
Qingfengteng (Sinomenii Caulis)	[0, 0, 0, 0, 1, 0, 1, 0, 1, 0, 0, 0, 0, 0, 0, 0, 0, 0, 0, 0, 0, 1, 1, 0, 0]

The 23-dimensional vectors from left to right represent: cold, hot, warm, cool, neutral, sour, bitter, sweet, pungent, salty, lung, pericardium, heart, large intestine, triple energizer, small intestine, stomach, gallbladder, bladder, spleen, liver, kidney, and toxicity. These attributes are described with modifying words to indicated their degree; for example, "slightly cold" "cold" and "very cold" are represented as  $2^{-1}$  (0.5),  $2^0$  (1), and  $2^1$  (2), respectively. If the attribute is absent, it is denoted by 0. The Guijing (归经, meridian tropism) attribute is binary quantified, with 1 indicating the presence of the attribute and 0 indicating its absence.

### 2.3 Model training and target prediction

The herb-target training dataset was constructed based on the data collected in Section 2.1 and randomly split into training (43 513 pairs), validation (5 439 pairs), and test (5 439 pairs) sets according to an 8 : 1 : 1 ratio. As shown in Figure 2, the impact of various hyperparameters was tested on the model's performance. Among them, the learning rate and batch size are the top two hyperparameters that most significantly affect the model's performance. By adjusting these two parameters and using 5-fold cross-validation with the area under the receiver operating characteristic curve (AUC) as the metric, the results are illustrated in Figure 3. We found that AUC had reached its maximum value when the learning rate was 0.0001 and the batch size was 64. All the hyperparameters of TCMHTI are summarized in Table 3.

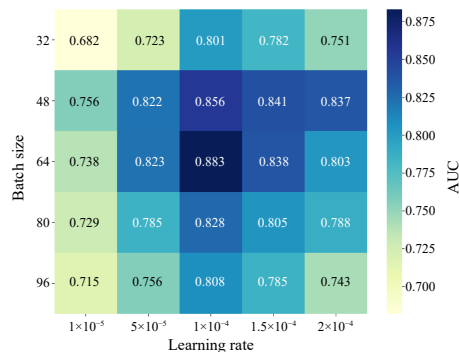


Figure 3 AUC heatmap for learning rate and batch size

Table 3 Hyperparameters of the TCMHTI model

Hyperparameter	Optimal value
Dimension of herb vectors	23
Dimension of target vectors	100
Number of attention heads	8
Number of encoder/decoder layers	3
Hidden size of decoder	64
Hidden size of Bi-LSTM	128
Batch size	64
Learning rate	0.000 1
Training epoch	100

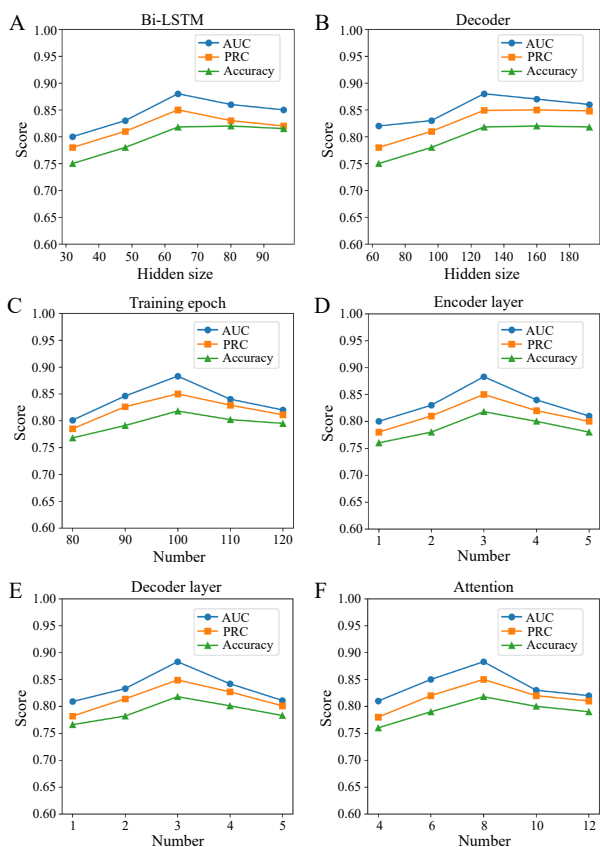


Figure 2 The impact of different hyperparameters on model performance

A, hidden size of Bi-LSTM. B, hidden size of decoder. C, training epoch. D, number of encoder layers. E, number of decoder layers. F, number of attention heads.

Classical binary classification evaluation metrics, including the AUC, the precision-recall curve (PRC), and accuracy, were used to assess model performance [17]. Then, the TCMHTI model was compared with various machine learning and deep learning models, such as support vector machines (SVM) [18], L2-logistic (L2) regression [19], k-nearest neighbors (KNN) [20], random

forests (RF) [21], and TransformerCPI [13]. Based on the completed model training, the collected QFJBD-target prediction set was input into the TCMHTI model to predict the interaction relationships between QFJBD and RA targets.

### 2.4 Network pharmacology analysis

**2.4.1 Screening of intersection targets** RA targets were screened from DisGeNET (score\_gda  $\geq$  0.1; <https://disgenet.com/>) and GeneCards (relevance\_score  $\geq$  10; <https://www.genecards.org/>) websites. QFJBD herb-targets were collected from TCMSP. The intersection of RA and QFJBD targets was identified as the targets through which QFJBD acts on RA. It is noteworthy that in Section 2.1, we adopted more stringent criteria (DisGeNET: score\_gda  $\geq$  0.5; GeneCards: relevance\_score  $\geq$  40) to screen RA targets for the TCMHTI method. This is because when classical network pharmacology methods applied the same screening criteria as TCMHTI, only 10 overlapping targets were obtained after intersecting the screened RA targets with QFJBD targets. An insufficient number of targets (only 10) for Gene Ontology (GO) and Kyoto Encyclopedia of Genes and Genomes (KEGG) enrichment analysis would lead to unreliable results. Therefore, classical network pharmacology methods appropriately lowered the screening criteria in RA target selection to avoid overlooking potential targets.

**2.4.2 PPI network analysis** The targets predicted by the TCMHTI model in Section 2.3 and the intersection targets screened in Section 2.4.1 were separately uploaded to the Search Tool for the Retrieval of Interacting Genes/Proteins (STRING) database. The species was set to “Homo sapiens”, and the minimum interaction threshold was set to “medium confidence” (0.4) to obtain PPI relationships. The results were imported into Cytoscape software (v3.7.1) for PPI network development and topological parameter analysis. Targets were ranked based on degree values in descending order to identify the core targets. The core targets predicted by the model were compared with those from the intersection of targets.

**2.4.3 GO function and KEGG pathway enrichment analysis** To explore the mechanisms of action of TCMHTI-predicted targets in the treatment of RA with QFJBD, and to verify the superiority of the TCMHTI model over the classical network pharmacology approach, both the intersection targets from Section 2.4.1 and the TCMHTI-predicted targets were subjected to GO and KEGG enrichment analysis using the Database for Annotation, Visualization, and Integrated Discovery (DAVID) database. Statistically significant terms were identified with a threshold of  $P$  value  $< 0.05$ . The top 10 entries ranked by  $P$  value in ascending order were selected to generate GO bar charts and KEGG bubble charts by a bioinformatics platform (<https://www.bioinformatics.com.cn/>). Then, the results of both methods were compared.

## 2.5 Model interpretation

Although deep learning was recognized as a black-box algorithm, the visualization experiments were conducted to explain the decision-making process of the model. Gradient-weighted class activation mapping (Grad-CAM) was used to visualize the decision-making process of deep learning models [22]. It generated an attention map by calculating the gradient of the target class, showing the feature regions that the model focused on when making predictions. In our experiments, we focused on which herb attributes had the greatest impact on the model's predictions of herb-target interactions. For each herb-target pair, the gradient values of the model's predicted probability with respect to the input attribute features were calculated. Larger absolute gradient values indicated a stronger contribution of the corresponding attribute to the prediction. Subsequently, the positive group (herb-target pairs predicted to interact) and the negative group (non-interacting pairs) were statistically compared by calculating the average gradient importance scores for each attribute within both groups. Finally, differences in critical attributes were intuitively visualized through bar charts.

## 2.6 Molecular docking and literature validation

Based on the results from Sections 2.3 and 2.4, we identified the core targets predicted by TCMHTI and their associated signaling pathways. The main active components of the five herbs in QFJBD were identified by consulting the *Pharmacopoeia of the People's Republic of China 2020* [23]. Molecular docking experiments were conducted between these components and core targets using AutoDock v4.2.6, with binding affinity as the primary evaluation metric. A docking score  $\leq -5.0$  kcal/mol was considered indicative of strong binding activity, based on established criteria for ligand-receptor interactions [24]. Additionally, to validate the accuracy of TCMHTI predictions, we systematically reviewed relevant literature to identify wet-lab experimental evidence demonstrating that the active components predicted by TCMHTI bind to target proteins and exert therapeutic effects on RA. The overall research workflow is illustrated in Figure 4.

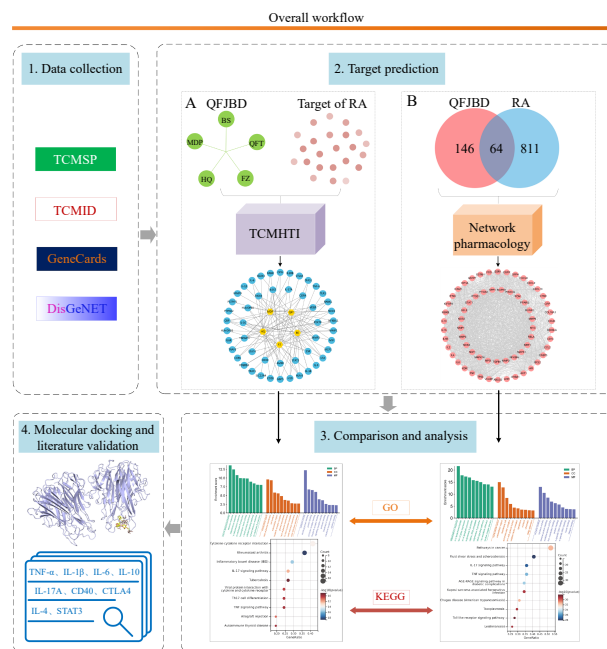


**Figure 4** Overall workflow of the TCMHTI model development and validation for predicting herb-target interactions in QFJBD treatment of RA

Step 1, collection of herb and target data. Step 2, two methods for predicting targets of QFJBD in treating RA. A, prediction of relevant targets using the TCMHTI model. B, screening of relevant targets through network pharmacology. Step 3, comparison and analysis of GO and KEGG results from both methods. Step 4, molecular docking and literature validation of core targets predicted by the TCMHTI model.

## 3 Results and analysis

### 3.1 Performance comparison between the TCMHTI model and other models

The performance of the trained TCMHTI model was compared with other machine learning models,



**3.3.3 Results of comparative analysis of GO and KEGG enrichment** GO enrichment analysis of the 49 targets predicted by the TCMHTI model revealed that these targets are primarily involved in biological processes such as cellular response to lipopolysaccharide, immune response, inflammatory response, regulation of inflammatory cytokine expression, and regulation of NF-κB transcription factor activity (Figure 7). In contrast, GO enrichment analysis of the intersection targets screened by classical network pharmacology showed the

involvement in biological processes, including inflammatory response, cellular response to lipopolysaccharide, regulation of gene expression, regulation of apoptosis process, and regulation of transcription from RNA polymerase II promoter. Compared with the TCMHTI model, the classical approach lacked processes such as immune response, regulation of IL-6 expression, and regulation of NF-κB transcription factor activity, which have been proven to be closely related to RA [25].

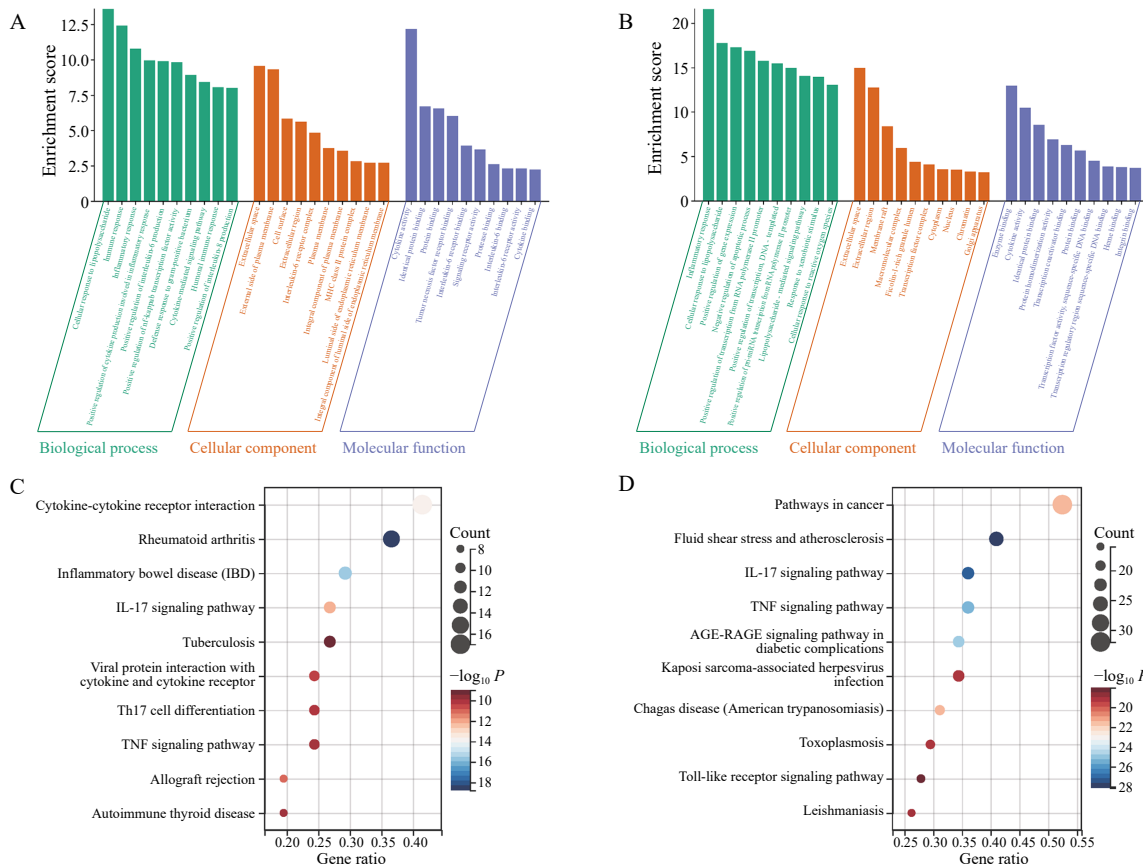


**Figure 7** Histogram of GO enrichment analysis and Bubble plot of KEGG enrichment analysis

A, GO enrichment analysis of targets predicted by TCMHTI model. B, GO enrichment analysis of targets from network pharmacology screening. C, KEGG enrichment analysis of targets predicted by TCMHTI model. D, KEGG enrichment analysis of targets from network pharmacology screening.

The results of the comparison of KEGG enrichment analysis showed that pathways ranked by ascending  $P$  value for the 64 intersection targets identified through classical network pharmacology, including fluid shear stress and atherosclerosis, advanced glycation end products-receptor for advanced glycation end products (AGE-RAGE) signaling pathway in diabetic complications, pathways in cancer, Chagas disease, toxoplasmosis, Kaposi sarcoma-associated herpesvirus infection, and leishmaniasis, which have weak associations with RA. In contrast, the top-ranked pathways involving targets predicted by TCMHTI included RA, inflammatory bowel disease, cytokine-cytokine receptor interaction, T helper 17 (Th17) cell differentiation, and NF-κB signaling pathway.

The study also found that signaling pathways such as IL-17 and TNF were common to both methods, suggesting that these might be the key signaling pathways for the treatment of RA (Figure 7).

**3.4 Interpretation of the TCMHTI model**

We chose Fuzi (Aconiti Lateralis Radix Praeparata) and Qingfengteng (Sinomenii Caulis) from QFJBD as examples. As illustrated in Figure 8, the gradient weights were mapped to the 23-dimensional features of the herbs. For different herb-target pairs, the model focused on different herb features and correctly categorized herb-target pairs into interaction and non-interaction categories. For

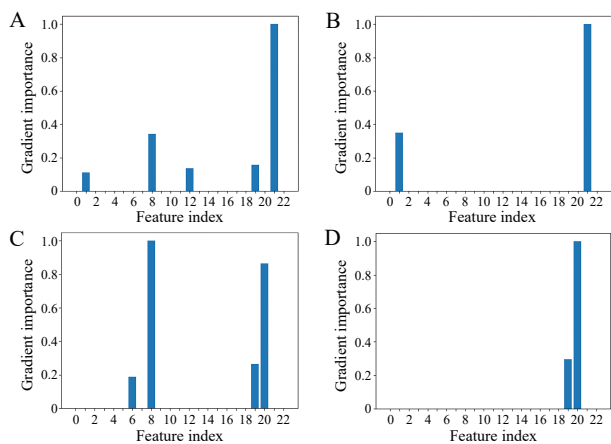


**Figure 8** Gradient weights of 23-dimensional features of the herbs

The feature index represents the 23-dimensional features of the herbs. A, Fuji (*Aconiti Lateralis Radix Praeparata*) interacting with CTLA4. B, Fuji (*Aconiti Lateralis Radix Praeparata*) not interacting with CD28. C, Qingfengteng (*Sinomenii Caulis*) interacting with CD40. D, Qingfengteng (*Sinomenii Caulis*) not interacting with CCL2.

example, in herb-target pairs with interactions (Fuji-CTLA4), the model noticed more herb features compared to herb-target pairs without interactions (Fuji-CD28). The TCMHTI model correctly captured the effect of the 23-dimensional features of herbs on the prediction results. This information is helpful in optimizing the model and informing the understanding of the relationship between the 23-dimensional features of herbs and their targets.

### 3.5 Results of molecular docking and literature validation

Based on the *Pharmacopoeia of the People's Republic of China 2020* [23], we systematically retrieved the active components of the five herbs in QFJBD. Key components, including paeoniflorin, paeonol, sinomenine, astragalus polysaccharide, calycosin-7-glucoside, and aconitine, were identified. For each herb, one to two components were selected based on their high abundance and documented pharmacological relevance, ensuring both representativeness and therapeutic utility. Molecular docking was then performed between these active components and the nine core targets predicted by the TCMHTI model using AutoDock. The binding energies calculated were recorded (Table 5), and the docking results were subsequently visualized (Figure 9). The results showed that most of the key active components of QFJBD bind well to the core targets.

The results of Section 3.3.3 indicated that most of the top 10 signaling pathways screened by classical network pharmacology are unrelated to RA. Specifically, the pathways identified as unrelated include fluid shear stress and atherosclerosis [26], AGE-RAGE signaling pathway in diabetic complications [27], cancer pathways [28], Chagas

**Table 5** Molecular docking binding energy of key active components and corresponding core targets

Component-target	Binding energy (kcal/mol)
Paeoniflorin-TNF- $\alpha$	-8.4
Paeoniflorin-IL-4	-7.2
Paeoniflorin-STAT3	-6.5
Paeoniflorin-IL-10	-7.0
Paeonol-IL-1 $\beta$	-4.2
Paeonol-IL-6	-4.9
Sinomenine-CD40	-7.2
Sinomenine-IL-17A	-6.7
Astragalus polysaccharide-IL-6	-5.5
Astragalus polysaccharide-TNF- $\alpha$	-6.2
Calycosin-7-glucoside-IL-10	-5.2
Aconitine-CTLA4	-6.7

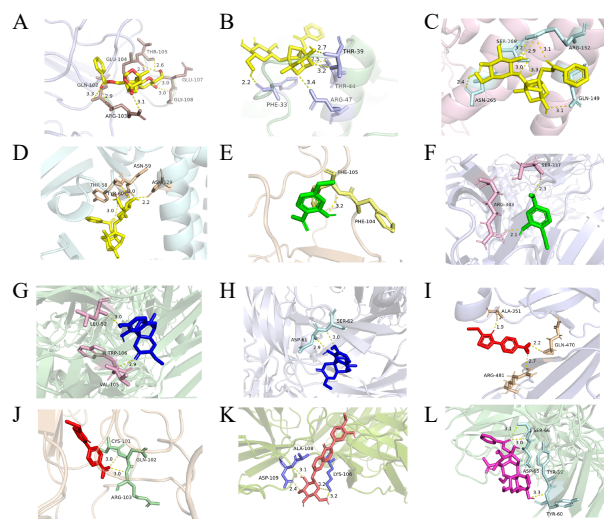


**Figure 9** Molecular docking visualization of active compounds from QFJBD with core RA targets

A, paeoniflorin-TNF- $\alpha$ . B, paeoniflorin-IL-4. C, paeoniflorin-STAT3. D, paeoniflorin-IL-10. E, paeonol-IL-1 $\beta$ . F, paeonol-IL-6. G, sinomenine-CD40. H, sinomenine-IL-17A. I, astragalus polysaccharide-IL-6. J, astragalus polysaccharide-TNF- $\alpha$ . K, calycosin-7-glucoside-IL-10. L, aconitine-CTLA4.

disease (American trypanosomiasis) [29], toxoplasmosis [30], Kaposi's sarcoma-associated herpesvirus infection [31], and leishmaniasis [32]. While these pathways are significant within their respective contexts, they are not directly correlated with the pathogenesis of RA. In contrast, the top 10 signaling pathways predicted by the TCMHTI model include RA, inflammatory bowel disease, cytokine-cytokine receptor interaction, Th17 cell differentiation, and NF- $\kappa$ B signaling pathway. Previous study reveals that RA and inflammatory bowel disease are both autoimmune diseases with similar pathogenesis mechanisms, involving complex interactions among immune inflammation, gut microecology, and genetic factors [33].

In RA, the overproduction of various cytokines leads to exacerbated inflammatory responses and tissue damage of the joints. One approach to treating RA is to alleviate inflammation by inhibiting pro-inflammatory factors such as IL-1 $\beta$  or blocking their receptors [25]. Th17 cells produce a spectrum of pro-inflammatory cytokines, including IL-17, IL-6, and TNF- $\alpha$ , which are essential factors in the immunopathogenesis of RA [34]. The NF- $\kappa$ B signaling pathway was key in chondrocyte inflammatory responses, leading to progressive extracellular matrix damage and cartilage destruction [35]. The two common pathways, IL-17 and TNF signaling pathways, are hypothesized to be critical for treating RA. The IL-17 pathway is involved in the pathogenesis of many human autoimmune and inflammatory diseases, including RA and psoriasis. It plays a key role in the destruction processes of tissue in some diseases, such as bone and cartilage

erosion in RA [36]. The TNF signaling pathway could have an adverse effect on certain chemokines and growth factors, resulting in higher expression levels of TNF- $\alpha$  in RA patients, thereby exacerbating inflammatory responses [37].

The results have been verified by previous scholarly findings, and they demonstrated that the molecular pathways involved in the targets predicted by the TCMHTI model are more closely related to the process of RA, indicating that the TCMHTI model is more accurate at predicting disease targets compared with classical network pharmacology methods. Further literature review of the core targets predicted by the TCMHTI model revealed that the herbs of QFJBD could treat RA and related diseases through one or more of the nine core targets (Table 6).

**Table 6** Literature validation of QFJBD-target relationship

Herb	Model	Target	Description
Baishao (Paeoniae Radix Alba)	L929 cell	TNF- $\alpha$	It shows the effects of TNF- $\alpha$ on L929 cells <i>in vitro</i> [38]
	Kunming mice, Munich-Wistar rats	STAT3, IL-10	It could regulate the STAT3 pathway on Munich-Wistar rats <i>in vivo</i> and upregulate IL-10 on Kunming mice <i>in vivo</i> [39]
	Kunming mice	IL-4	It could increase the levels of IL-4 in Kunming mice <i>in vivo</i> [40]
Mudanpi (Moutan Cortex)	Primary HFLS-RA cell, DBA/1 mice	IL-1 $\beta$ , IL-6	It could inhibit cytokines levels of IL-1 $\beta$ and IL-6 on HFLS-RA cells <i>in vitro</i> and DBA/1 mice <i>in vivo</i> [41]
Huangqi (Astragali Radix)	RSC-364, RA-FLS cell	IL-6, TNF- $\alpha$	IL-6 and TNF- $\alpha$ were significantly decreased after Huangqi (Astragali Radix) on RSC-364 and RA-FLS cells <i>in vitro</i> [42]
	RAW 264.7 macrophage cell	IL-10	IL-10 was evaluated after treating Huangqi (Astragali Radix) on RAW 264.7 macrophage cells <i>in vitro</i> [43]
Fuzi (Aconiti Lateralis Radix Praeparata)	Hepa1-6, C57BL/6 mice	CTLA4	It modulated CTLA4 on Hepa1-6 cells <i>in vitro</i> and C57BL/6 mice <i>in vivo</i> [44]
Qingfengteng (Sinomenii Caulis)	PBMCs cell	CD40	Its effect on CD40 was validated on PBMCs cells <i>in vitro</i> [45]
	SD rats, PBMCs cell	IL-17A	The effect of it on IL-17A was determined on SD rats <i>in vivo</i> and PBMCs cells <i>in vitro</i> [46]

L929, mouse connective tissue fibroblast cell line L929. HFLS-RA, human fibroblast-like synoviocytes from RA patient. RSC-364, rat synovial cell line 364. RA-FLS, RA fibroblast-like synoviocytes. RAW 264.7, murine macrophage cell line RAW 264.7. PBMCs, peripheral blood mononuclear Cells. SD, Sprague-Dawley.

## 4 Discussion

To explore the therapeutic mechanisms of QFJBD in RA, we proposed an improved TCMHTI model based on the Transformer architecture. The TCMHTI model was then used to predict herb-target interactions. When compared with several traditional machine learning methods and DTI models on the collected herb-target dataset, the TCMHTI model demonstrated significant advantages.

The TCMHTI model predicted nine core targets, including TNF- $\alpha$ , IL-1 $\beta$ , IL-6, IL-10, IL-17A, CD40, CTLA4, IL-4, and STAT3, for QFJBD in RA treatment. Research has shown that TNF- $\alpha$  and IL-1 $\beta$  are crucial in cell damage and inflammation in RA [47]. IL-17 functions as a pro-inflammatory cytokine exacerbating joint damage in

arthritis, whereas IL-10 and IL-4 contribute to protective immunoregulation that may limit bone erosion [48-50]. IL-6 can stimulate the Th17 pathway, leading to fibrosis and inflammatory responses [51]. STAT3 signaling propagates inflammation and osteoclast activity, constituting a critical therapeutic target for preventing joint destruction in RA [52]. CD40 is involved in various pathological processes of RA, including immune response, destruction of articular cartilage and bone, and the inflammatory cytokine network in synovial tissue [53]. CTLA4 is a protein receptor on T cells that acts as an immune checkpoint, downregulating the immune system. Blocking CTLA4 significantly affects several other cell types involved in RA pathophysiology [54].

Unlike classical network pharmacology, which identified 64 targets with limited relevance to RA, the TCMHTI

model prioritized disease-specific signaling pathways. Only two overlapping pathways, IL-17 and TNF signaling pathways, were shared, and both are recognized as key signaling pathways for treating RA. Further validation of the core targets predicted by the TCMHTI model, based on literature, demonstrated that QFJBD can treat RA through these core targets. Molecular docking results demonstrated favorable binding affinities between active components in QFJBD and the nine core targets, while literature review identified wet-lab experimental evidence supporting the RA-interventional effects of these component-target interactions, thereby validating the accuracy of TCMHTI predictions through both computational and empirical approaches. This suggests that the TCMHTI model exhibits superior accuracy in identifying disease-associated targets compared with classical network pharmacology, thereby opening new avenues for mechanistic exploration and therapeutic optimization of TCM in complex diseases like RA.

However, this study also has several limitations. As a deep learning model, TCMHTI lacks interpretability and cannot explain why specific herbs interact with certain targets. Additionally, the model is unable to predict interactions between unknown herbs and unknown targets. Although we validated our predictions through a comprehensive literature review, we recognize the importance of conducting our own experimental validations to strengthen our findings. In future work, we will optimize the model and conduct empirical experiments to further validate our results.

## 5 Conclusion

This study used the TCMHTI model to predict potential targets of QFJBD in treating RA. The network pharmacology analysis of the TCMHTI-predicted targets indicates that QFJBD may primarily exert its therapeutic effects on RA by influencing the expression of target proteins such as TNF- $\alpha$ , IL-1 $\beta$ , and STAT3. These findings provide a novel framework for bridging traditional herbal knowledge with precision medicine, offering actionable insights for developing targeted TCM therapies against diseases.

## Fundings

General Program of the National Natural Science Foundation of China (82474352), and Natural Science Foundation of Hunan Province (2023JJ60124).

## Competing interests

Changsong DING is an editorial board member for *Digital Chinese Medicine* and was not involved in the editorial review or the decision to publish this article. All authors declare that there are no competing interests.

## References

- [1] FINCKH A, GILBERT B, HODKINSON B, et al. Global epidemiology of rheumatoid arthritis. *Nature Reviews Rheumatology*, 2022, 18(10): 591–602.
- [2] WANG Y, CHEN SJ, DU KZ, et al. Traditional herbal medicine: Therapeutic potential in rheumatoid arthritis. *Journal of Ethnopharmacology*, 2021, 279: 114368.
- [3] LI X, LIN Y, CHEN XJ, et al. Clinical efficacy study of Qingfu Juanbi Decoction in treating rheumatoid arthritis with syndrome of cold-dampness arthralgia. *China Journal of Traditional Chinese Medicine and Pharmacy*, 2019, 34(1): 403–407.
- [4] PAUL SM, MYTELKA DS, DUNWIDDIE CT, et al. How to improve R&D productivity: the pharmaceutical industry's grand challenge. *Nature Reviews Drug Discovery*, 2010, 9(3): 203–214.
- [5] HOPKINS AL. Network pharmacology: the next paradigm in drug discovery. *Nature Chemical Biology*, 2008, 4(11): 682–690.
- [6] WANG X, WANG ZY, ZHENG JH, et al. TCM network pharmacology: a new trend towards combining computational, experimental and clinical approaches. *Chinese Journal of Natural Medicines*, 2021, 19(1): 1–11.
- [7] LI S, ZHANG B. Traditional Chinese medicine network pharmacology: theory, methodology and application. *Chinese Journal of Natural Medicines*, 2013, 11(2): 110–120.
- [8] BAGHERIAN M, SABETI E, WANG K, et al. Machine learning approaches and databases for prediction of drug-target interaction: a survey paper. *Briefings in Bioinformatics*, 2021, 22(1): 247–269.
- [9] LEE I, KEUM J, NAM H. DeepConv-DTI: prediction of drug-target interactions via deep learning with convolution on protein sequences. *PLoS Computational Biology*, 2019, 15(6): e1007129.
- [10] DENG L, DING CS, HUANG XD, et al. Quantitative study on medicinal properties of traditional Chinese medicine based on BP neural network. *Chinese Traditional and Herbal Drugs*, 2020, 51(16): 4277–4283.
- [11] VASWANI A, SHAZEER N, PARMAR N, et al. Attention is all you need. arXiv, 2017. doi: 10.48550/arXiv.1706.03762.
- [12] MEDSKER L, JAIN LC. *Recurrent Neural Networks: Design and Applications*. Boca Raton: CRC Press, 1999.
- [13] CHEN LF, TAN XQ, WANG DY, et al. TransformerCPI: improving compound-protein interaction prediction by sequence-based deep learning with self-attention mechanism and label reversal experiments. *Bioinformatics*, 2020, 36(16): 4406–4414.
- [14] GREFF K, SRIVASTAVA RK, KOUTNÍK J, et al. LSTM: a search space odyssey. *IEEE Transactions on Neural Networks and Learning Systems*, 2017, 28(10): 2222–2232.
- [15] RU JL, LI P, WANG JN, et al. TCMSP: a database of systems pharmacology for drug discovery from herbal medicines. *Journal of Cheminformatics*, 2014, 6: 13.
- [16] CHURCH KW. Word2Vec. *Natural Language Engineering*, 2017, 23(1): 155–162.
- [17] RAINIO O, TEUHO J, KLÉN R. Evaluation metrics and statistical tests for machine learning. *Scientific Reports*, 2024, 14(1): 6086.

- [18] GUENTHER N, SCHONLAU M. Support vector machines. *The Stata Journal*, 2016, 16(4): 917-937.
- [19] CUCCHIARA A, HOSMER D, LEMESHOW S. Applied logistic regression. *Technometrics*, 1992, 34(3): 358.
- [20] ZHANG ZH. Introduction to machine learning: k-nearest neighbors. *Annals of Translational Medicine*, 2016, 4(11): 218.
- [21] RIGATTI SJ. Random forest. *Journal of Insurance Medicine*, 2017, 47(1): 31-39.
- [22] SELVARAJU RR, COGSWELL M, DAS A, et al. Grad-CAM: visual explanations from deep networks via gradient-based localization. 2017 IEEE International Conference on Computer Vision (ICCV). IEEE, 2017: 618-626.
- [23] COMMITTEE NP. Chinese Pharmacopoeia: Volume I. Beijing: China Medical Science Press, 2020.
- [24] PAGADALA NS, SYED K, TUSZYNSKI J. Software for molecular docking: a review. *Biophysical Reviews*, 2017, 9(2): 91-102.
- [25] ALAM J, JANTAN I, BUKHARI SNA. Rheumatoid arthritis: recent advances on its etiology, role of cytokines and pharmacotherapy. *Biomedicine & Pharmacotherapy*, 2017, 92: 615-633.
- [26] CUNNINGHAM KS, GOTLIEB AI. The role of shear stress in the pathogenesis of atherosclerosis. *Laboratory Investigation*, 2005, 85(1): 9-23.
- [27] RAMASAMY R, YAN SF, SCHMIDT AM. Receptor for AGE (RAGE): signaling mechanisms in the pathogenesis of diabetes and its complications. *Annals of the New York Academy of Sciences*, 2011, 1243: 88-102.
- [28] VOGELSTEIN B, KINZLER KW. Cancer genes and the pathways they control. *Nature Medicine*, 2004, 10(8): 789-799.
- [29] ECHEVERRIA LE, MORILLO CA. American trypanosomiasis (chagas disease). *Infectious Disease Clinics of North America*, 2019, 33(1): 119-134.
- [30] SMITH NC, GOULART C, HAYWARD JA, et al. Control of human toxoplasmosis. *International Journal for Parasitology*, 2021, 51(2/3): 95-121.
- [31] SCHULZ TF, CESARMAN E. Kaposi sarcoma-associated herpesvirus: mechanisms of oncogenesis. *Current Opinion in Virology*, 2015, 14: 116-128.
- [32] TORRES-GUERRERO E, QUINTANILLA-CEDILLO MR, RUIZ-ESMENJAUD J, et al. Leishmaniasis: a review. *F1000Research*, 2017, 6: 750.
- [33] CHEN Y, CHEN L, XING CS, et al. The risk of rheumatoid arthritis among patients with inflammatory bowel disease: a systematic review and meta-analysis. *BMC Gastroenterology*, 2020, 20(1): 192.
- [34] AZIZI G, JADIDI-NIARAGH F, MIRSHAFIEY A. Th17 Cells in immunopathogenesis and treatment of rheumatoid arthritis. *International Journal of Rheumatic Diseases*, 2013, 16(3): 243-253.
- [35] ROMAN-BLAS JA, JIMENEZ SA. NF- $\kappa$ B as a potential therapeutic target in osteoarthritis and rheumatoid arthritis. *Osteoarthritis and Cartilage*, 2006, 14(9): 839-848.
- [36] HU Y, SHEN F, CRELLIN NK, et al. The IL-17 pathway as a major therapeutic target in autoimmune diseases. *Annals of the New York Academy of Sciences*, 2011, 1217: 60-76.
- [37] VARFOLOMEEV E, GONCHAROV T, MAECKER H, et al. Cellular inhibitors of apoptosis are global regulators of NF- $\kappa$ B and MAPK activation by members of the TNF family of receptors. *Science Signaling*, 2012, 5(216): ra22.
- [38] LAI XY, WEI J, DING XH. Paeoniflorin antagonizes TNF- $\alpha$ -induced L929 fibroblastoma cells apoptosis by inhibiting NF- $\kappa$ B p65 activation. Dose-response, 2018, 16(2): 1559325818774977.
- [39] ZHANG LL, WEI W. Anti-inflammatory and immunoregulatory effects of paeoniflorin and total glucosides of paeony. *Pharmacology & Therapeutics*, 2020, 207: 107452.
- [40] WANG C, YUAN J, WU HX, et al. Paeoniflorin inhibits inflammatory responses in mice with allergic contact dermatitis by regulating the balance between inflammatory and anti-inflammatory cytokines. *Inflammation Research*, 2013, 62(12): 1035-1044.
- [41] ZHAI KF, DUAN H, LUO L, et al. Protective effects of paeonol on inflammatory response in IL-1 $\beta$ -induced human fibroblast-like synoviocytes and rheumatoid arthritis progression via modulating NF- $\kappa$ B pathway. *Inflammopharmacology*, 2017. doi: 10.1007/s10787-017-0385-5.
- [42] MENG QL, DU XZ, WANG HL, et al. *Astragalus* polysaccharides inhibits cell growth and pro-inflammatory response in IL-1 $\beta$ -stimulated fibroblast-like synoviocytes by enhancement of autophagy via PI3K/AKT/mTOR inhibition. *Apoptosis*, 2017, 22(9): 1138-1146.
- [43] LI JX, XU L, SANG R, et al. Immunomodulatory and anti-inflammatory effects of total flavonoids of *Astragalus* by regulating NF- $\kappa$ B and MAPK signalling pathways in RAW 264.7 macrophages. *Die Pharmazie*, 2018, 73(10): 589-593.
- [44] WEI ZR, WANG WJ, WANG SJ, et al. Exploration into the immune mechanism and detoxication of aconitine combined with polycytidylic acid on antitumor. *Journal of Lanzhou University (Natural Sciences)*, 2023, 59(2): 248-255.
- [45] ZHAO Y, LI J, YU KQ, et al. Sinomenine inhibits maturation of monocyte-derived dendritic cells through blocking activation of NF- $\kappa$ B. *International Immunopharmacology*, 2007, 7(5): 637-645.
- [46] TONG B, YU JT, WANG T, et al. Sinomenine suppresses collagen-induced arthritis by reciprocal modulation of regulatory T cells and Th17 cells in gut-associated lymphoid tissues. *Molecular Immunology*, 2015, 65(1): 94-103.
- [47] MATEEN S, SHAHZAD S, AHMAD S, et al. Cinnamaldehyde and eugenol attenuates collagen induced arthritis via reduction of free radicals and pro-inflammatory cytokines. *Phytomedicine*, 2019, 53: 70-78.
- [48] LUO Q, LIU YJ, SHI K, et al. An autonomous activation of interleukin-17 receptor signaling sustains inflammation and promotes disease progression. *Immunity*, 2023, 56(9): 2006-2020. e6.
- [49] HAIKAL SM, ABDELTAWAB NF, RASHED LA, et al. Combination therapy of mesenchymal stromal cells and interleukin-4 attenuates rheumatoid arthritis in a collagen-induced murine model. *Cells*, 2019, 8(8): 823.
- [50] KATSIKIS PD, CHU CQ, BRENNAN FM, et al. Immunoregulatory role of interleukin 10 in rheumatoid arthritis. *The Journal of Experimental Medicine*, 1994, 179(5): 1517-1527.
- [51] PANDOLFI F, FRANZA L, CARUSI V, et al. Interleukin-6 in rheumatoid arthritis. *International Journal of Molecular*

Sciences, 2020, 21(15): 5238.

[52] OIKE T, SATO Y, KOBAYASHI T, et al. Stat3 as a potential therapeutic target for rheumatoid arthritis. *Scientific Reports*, 2017, 7(1): 10965.

[53] RAYCHAUDHURI S, REMMERS EF, LEE AT, et al. Common

variants at CD40 and other loci confer risk of rheumatoid arthritis. *Nature Genetics*, 2008, 40(10): 1216-1223.

[54] CUTOLO M, SULLI A, PAOLINO S, et al. CTLA-4 blockade in the treatment of rheumatoid arthritis: an update. *Expert Review of Clinical Immunology*, 2016, 12(4): 417-425.

## TCMHTI: 基于 Transformer 的青附蠲痹汤治疗类风湿关节炎的中药-靶点相互作用预测模型

梁振忠<sup>a</sup>, 丁长松<sup>a, b\*</sup>

a. 湖南中医药大学信息科学与工程学院, 湖南长沙 410208, 中国

b. 湖南中医药大学中医药大数据分析实验室, 湖南长沙 410208, 中国

**【摘要】目的** 采用改进的 Transformer 模型预测青附蠲痹汤 (QFJBD) 治疗类风湿关节炎 (RA) 的潜在靶点, 探究 QFJBD 治疗 RA 的网络药理机制。**方法** 首先, 构建基于 Transformer 改进的中药-靶点的相互作用预测模型 (TCMHTI)。采用受试者工作特征曲线下面积 (AUC)、精确率-召回率曲线 (PRC) 和准确率三项指标评价, 将 TCMHTI 模型与基线模型进行性能比较。随后, 基于预测靶点构建蛋白质-蛋白质相互作用 (PPI) 网络, 并根据度值排名确定前 9 个节点为核心靶点, 利用 TCMHTI 预测靶点与网络药理学方法鉴定的靶点分别进行基因本体论 (GO) 功能注释和京都基因与基因组百科全书 (KEGG) 通路富集分析, 并将富集分析结果进行对比。最后, 通过分子对接和文献查阅对 TCMHTI 预测的核心靶点进行验证。**结果** TCMHTI 模型的 AUC 值为 0.883, PRC 值为 0.849, 准确率为 0.818, 预测出 49 个 QFJBD 治疗 RA 的潜在靶点并筛选出 9 个核心靶点: 肿瘤坏死因子 (TNF)- $\alpha$ 、白细胞介素 (IL)-1 $\beta$ 、IL-6、IL-10、IL-17A、簇抗原分化簇 40 (CD40)、细胞毒性 T 淋巴细胞相关抗原-4 (CTLA4)、IL-4 及信号转导和转录激活因子-3 (STAT3)。富集分析显示, TCMHTI 模型预测出 49 个靶点, 富集到更多与 RA 直接相关的通路; 而经典网络药理学虽得到 64 个靶点, 但富集的通路与 RA 关联性较弱。分子对接显示 QFJBD 中的活性分子与 RA 靶点有良好的结合能, 而文献调研结果也显示了 QFJBD 可以通过 9 个核心靶点来治疗 RA。**结论** TCMHTI 模型比网络药理学方法具有更高的准确性, 表明 QFJBD 主要通过影响 TNF- $\alpha$ 、IL-1 $\beta$ 、IL-6 等靶点及多个信号通路来发挥对 RA 的治疗作用。本研究为传统中医药与精准医学相结合提供了一个新的框架, 并为开发针对疾病的中医靶向疗法提供了可行的见解。

**【关键词】** Transformer; 青附蠲痹汤; 类风湿关节炎; 深度学习; 网络药理学